Atmospheric
Chemistry
and Physics
Discussions

Open Access

Long-term change in the contributions of various source regions to surface ozone over Japan

Tatsuya Nagashima[1], Kengo Sudo[2,3], Hajime Akimoto[1], Junichi Kurokawa[4], and Toshimasa Ohara[1]

[1]National Institute for Environmental Studies, Tsukuba, Japan

[2]Graduate School of Environmental Studies, Nagoya University, Nagoya, Japan

[3]Frontier Research Center for Global Change, Yokohama, Japan

[4]Asia Center for Air Pollution Research, Niigata, Japan

Correspondence to: T. Nagashima (nagashima.tatsuya@nies.go.jp)

Abstract

The relative contributions of various source regions to the long-term (1980–2005) increasing trend in surface ozone (O_3) over Japan were estimated by a series of tracer-tagging simulations using a global chemical transport model. The model well simulated the observed increasing trend of surface O_3 including its seasonal variation and geographical features in Japan and demonstrated the relative roles of different source regions in forming this trend. Most of the simulated increasing trend of surface O_3 over Japan (~97 %) was explained as the sum of trends in contributions of different regions to photochemical O_3 production. The increasing trend in O_3 produced in China accounted for 36 % of the total increasing trend and those in the other northeast Asian regions (the Korean Peninsula, coastal regions in East Asia, and Japan) each accounted for about 12–15 %. Furthermore, the contributions of O_3 created in the entire free troposphere and in West, South, and Southeast Asian regions also increased; and their increasing trends accounted for 16 and 7 % of the total trend, respectively. The impact of interannual variations in climate, in methane concentration, and in emission of O_3 precursors from different source regions on the relative contributions of O_3 created in each region estimated above was also investigated. The variation of climate and the increase in methane concentration together caused the increase of photochemical O_3 production in several regions, and represented about 19 % of the total increasing trend of surface O_3 over Japan. The increase in emission of O_3 precursors in China caused an increase of photochemical O_3 production not only in China itself but also in the other northeast Asian regions and accounted for about 46 % of the total increase in surface O_3 over Japan. Similarly, the relative impact of O_3 precursor emission changes in the Korean Peninsula and Japan were estimated as about 16 and 4 % of the total increasing trend, respectively. The O_3 precursor emission change in regions other than northeast Asia caused increases in surface O_3 over Japan mainly through increasing photochemical O_3 production in West, South, and Southeast Asia and the free troposphere, and accounted for about 16 % of the total.

Atmospheric
Chemistry
and Physics
Discussions

1 Introduction

Tropospheric ozone (O_3) plays multiple roles in the atmosphere. O_3 itself is an oxidant and photodissociates to generate the hydroxyl radical which strongly oxidizes many atmospheric compounds including various air pollutants and thus removes them from the atmosphere. In contrast, high levels of O_3 are a major air pollutant due to adverse effects on human health, natural vegetation, and agricultural produce (Wang and Mauzerall, 2004; Mauzerall et al., 2005; US EPA, 2006; Silva et al., 2013). Moreover, tropospheric O_3 is a major greenhouse gas in the atmosphere, and reduction of its amount was recently recognized as an effective measure to mitigate near-term climate change (UNEP and WMO, 2011; Shindell et al., 2012). Therefore, the spatial and temporal variations in tropospheric O_3 have been always a matter of scientific and public concern.

An increasing trend in tropospheric O_3 concentration has been observed during recent decades at many locations in East Asia including Taiwan (Chou et al., 2006; Chang and Lee; 2007; Li et al., 2010; Lin et al., 2010), mainland China (Lu and Wang, 2006; Ding et al., 2008; Xu et al., 2008; Wang et al., 2009; Zhang et al., 2014), and South Korea (Susaya et al., 2013; Lee et al., 2014; Seo et al., 2014). The increase rates of O_3 in those East Asian regions significantly vary depending on location and season in the range of about 0.3–3 ppbv/yr; however, the increases are generally larger than the trends in tropospheric O_3 for other regions in the world (Cooper et al., 2014). Japan is no exception, with an increasing trend found in various observations of O_3 over the past approximately 40 years. Routine ozonesonde measurements since 1970 at three Japanese sites of Sapporo (43° N), Tsukuba (36° N), and Kagoshima (32° N) showed an increasing trend of O_3 concentration in the lowermost troposphere up to about 1990 and relatively stable thereafter, with largest increase near the ground and discernible about 300 hPa height and below (Logan et al., 1999; Oltmans et al., 2006). With an air mass classification method based on backward air trajectories, Naja and Akimoto (2004) showed that a significant amount of the air masses reaching these ozonesonde sites in Japan spend substantial time over polluted regions in East Asia. The O_3 levels in these regionally polluted air masses increased from the 1970s to the 1990s, mainly due to large increases in nitrogen oxide ($NO_x = NO + NO_2$) emissions over China in the 1990s. Oltmans et al. (2013) analyzed a rather short period of data (1991–2010) obtained at the Ryori (39° N) surface site in north-eastern Japan and showed an increase into the mid-1990s followed by relatively little change. Other ground-based observations at a mountain site (Mt. Happo; 43° N, 1850 m asl) and three sites in the marine boundary layer along the west coast of Japan [Rishiri (45° N), Tappi (41° N), and Sado (38° N)], where few sources of pollutants exist nearby, obtained under the monitoring network of EANET (the Acid Deposition Monitoring Network in East Asia) also showed increasing trends of O_3 concentrations at least until the mid-2000s (Tanimoto, 2009; Tanimoto et al., 2009; Parrish et al., 2012).

In addition, analysis of long-term observations by the ambient air quality monitoring network mainly established in urban–suburban regions in Japan also showed continuous increases of surface O_3 from the mid-1980s until the present (Ohara and Sakata, 2003; Ohara et al., 2008; Kurokawa et al., 2009; MOE Japan, 2013; Wakamatsu et al., 2013; Akimoto et al., 2015). However, simultaneous observations of O_3 precursors such as NO_x and non-methane hydrocarbons (NMHCs) by this monitoring network revealed their decreasing trends in the same period (MOE Japan, 2013), which seemed inconsistent with the increasing trend of O_3 over Japan. These observed features of O_3-related atmospheric species in Japan suggest that there should be an influence of transboundary transport from outside of Japan on the recent increasing trend in O_3. The influence of transboundary transport on surface O_3 in East Asia was examined in several studies (Sudo and Akimoto, 2007; Li et al., 2008; Nagashima et

86   al., 2010; Wang et al., 2011). Nagashima et al. (2010) demonstrated that the O_3 transported
87   from outside of Japan accounted for more than 70 % of surface O_3 over Japan in the cold
88   season (October–March) during 2000–2005, and most was attributable to O_3 from distant
89   sources outside East Asia and from the stratosphere. In the warm season (April–September),
90   the contribution of domestically created O_3 in Japan to surface O_3 over Japan increased
91   significantly (about 20–40 %), the short range intra-regional transport of O_3 from other parts
92   of East Asia still contributed about 25 %, and long range inter-regional transport of O_3 from
93   outside East Asia and the stratosphere particularly in spring could account for about half of
94   surface O_3 over Japan.

95   Therefore, the influence of O_3 from source regions outside and inside East Asia and the
96   stratosphere should be considered to explain the cause of the increasing trend in surface O_3
97   over Japan. The rapid increase in O_3 precursor emissions in East Asia in recent decades
98   (Ohara et al., 2007; Kurokawa et al., 2013) was demonstrated as a major cause of the
99   increasing trend of springtime O_3 over Japan by comparing regional chemical transport model
100 (CTM) simulations of recent decades with and without the East Asian O_3 precursor emission
101 increases during the period (Kurokawa et al., 2009; Tanimoto et al., 2009). However, they
102 only showed the springtime O_3 case and it was unclear whether the relationship held in other
103 seasons. Moreover, the relative contributions of individual countries or regions in East Asia
104 have not been well examined, particularly concerning increased surface O_3 over Japan.

105 Here, we investigated the cause of the continuous increase in surface O_3 over Japan reported
106 in the above literature, focusing on the relative contributions of various source regions over
107 the globe, particularly the contributions of individual regions in East Asia, with a long-term
108 simulation of a global CTM using the tagged tracer method. Using the same model and
109 method, Nagashima et al. (2010) showed such relative contributions of regions inside and
110 outside East Asia on surface O_3 over Japan as average values for the early 2000s. The current
111 study investigated the temporal evolution of the relative contributions of each region for the
112 26 years of 1980–2005.

113

2   Methods

2.1   Model description

116 In this study, we employed a chemistry climate model (CCM), CHASER (Sudo et al., 2002),
117 developed for the atmospheric chemistry research in the troposphere. The basic setting of the
118 model was almost identical to that used by Nagashima et al. (2010). However, the horizontal
119 resolution was modified from T63 (about 1.9° by 1.9° grid spacing in longitude and latitude)
120 to T42 (about 2.8° by 2.8°), because longer simulation period was necessary than in the
121 previous study, and so the cost of computation was reduced in the present study by selecting
122 lower horizontal resolution. There were 32 vertical layers with the top layer set at
123 approximately 40 km altitude. A detailed tropospheric photochemistry consisted of 113
124 chemical reactions and 27 photodissociation involving O_3, HO_x, NO_x, methane (CH_4), CO and
125 NMHCs calculated the temporal evolution in the concentrations of 53 chemical species. The
126 gas and liquid phase oxidation of sulfur dioxide (SO_2) and dimethyl sulfide to form the sulfate
127 aerosol was also included in the model. The concentrations of O_3 and some nitrogen
128 compounds (NO_x, HNO_3, and N_2O_5) above the tropopause that should affect tropospheric
129 chemistry were assimilated into the monthly mean output data of stratospheric CCM, because
130 the version of CHASER used was unable to calculate several chemical processes, such as
131 halogen-related chemical reactions, which are indispensable for realistic representation of

132 such chemical compounds in the stratosphere. For the transport of chemical species, a semi-
133 Lagrangian advective transport scheme (Lin and Rood, 1996; van Leer, 1997) and vertical
134 convective transport associated with cumulus convection process were considered. The model
135 also included dry and wet deposition of chemical species.

136   In this study, we conducted tracer-tagging simulation by using two different setups (full-
137 chemistry and tracer-transport setups) of CHASER. The full-chemistry setup calculated the
138 actual temporal change in the concentration of chemical species through the abovementioned
139 chemical and physical processes and outputted the chemical production and loss tendencies of
140 O_3 and related species. Then, the tracer-transport setup used the outputted chemical
141 tendencies to calculate the temporal change in the concentration of hypothetical O_3 tracers. In
142 the following subsection, the calculation procedure is briefly described.

143

144 2.2 Outline of the numerical simulations

145 2.2.1 Forcings for long-term simulation

146   Long-term simulation was performed for the period 1980–2005. To drive the physical
147 properties of the model for this 26-year period, the temperature and horizontal wind velocities
148 in the model were assimilated into the National Center for Environmental Prediction/National
149 Center of Atmospheric Research (NCEP/NCAR) 6-hour reanalysis data (Kalnay et al., 1996)
150 of the corresponding year, and sea surface temperature and sea ice data of the Hadley Centre's
151 Sea Ice and Sea Surface Temperature (HadISST) data set (Rayner et al., 2003) were used in
152 the model.

153   The monthly mean stratospheric O_3 data of Akiyoshi et al. (2009) was used for the
154 assimilation above the tropopause for this period. These data were the output of a
155 stratospheric CCM simulation according to the hindcasting scenario for 1980–2004 (REF1
156 scenario) of the CCM validation activity (CCMVal) (Eyring et al., 2005), and included an
157 interannual variation (IAV) associated with the 11-year solar cycle and large declines after
158 1982 and 1991 due to the El Chichon and Pinatubo eruptions, respectively, in addition to a
159 continuous decreasing trend during the whole period. Although the simulated declines of
160 stratospheric O_3 due to the two large volcanic eruptions were somewhat overestimated, the
161 simulated IAVs in stratospheric O_3 reasonably well represented those observed with a total
162 ozone mapping spectrometer (TOMS) from satellites (Akiyoshi et al., 2009). Incidentally, the
163 stratospheric O_3 data of 2004 were used for 2005.

164   The long-term variation of the emissions of O_3 precursors (NO_x, CO, and NMHCs) and SO_2
165 were taken from multiple emission inventories. For anthropogenic emissions in Asia, the
166 Regional Emission inventory in ASia (REAS ver.1.2) (Ohara et al., 2007) was used for the
167 whole simulation period (1980–2005); the REAS emission data were available for each year
168 in the period. Kurokawa et al. (2009) used these emission data with a regional air quality
169 model representing well the interannual variability of surface O_3 over Japan for similar period
170 (1981–2005) to the present study. For anthropogenic emissions outside Asia, a combination of
171 three versions of EDGAR (Emission Database for Global Atmospheric Research) emission
172 data was used: EDGAR-HYDE (Van Aardenne et al., 2001) for 1980 and 1990; EDGAR v3.2
173 (Olivier and Berdowski, 2001) for 1990 and 1995; and EDGAR v3.2 Fast Track 2000
174 (FT2000) (Olivier and Berdowski, 2001) for 2000. Because several emission sectors
175 considered in EDGAR v3.2 were not considered in EDGAR-HYDE, the emissions for 1990
176 in EDGAR-HYDE were generally smaller than in EDGAR v3.2. Therefore, we used EDGAR

Atmospheric
Chemistry
and Physics
Discussions

Open Access

177   v3.2 data for 1990, and also scaled them to estimate emission data for 1980 rather than simply
178   using EDGAR-HYDE data for 1980. For that, we scaled EDGAR v3.2 data for 1990 so that
179   the ratio (r) of the difference between 1980 (f_1) and 1990 data (f_2) and their average in
180   EDGAR-HYDE [i.e., $r = (f_2 - f_1)/(f_1 + f_2)/2$] equaled the corresponding ratio (R) calculated
181   from 1990 data in EDGAR v3.2 (F_2) and 1980 data scaled from it (F_1) [i.e., $R = (F_2 - F_1)/(F_1 + F_2)/2$].
182     $F_2)/2$]. We calculated F_1 from the known values of f_1, f_2, and F_2 using the equation $r = R$.
183   Since EDGAR emission data were not available for each year but for every 10 or 5 years in
184   the simulation period, the emissions for intermediate years were interpolated, and FT2000
185   data used for years after 2000. The vegetation fire emission data developed in the REanalysis
186   of the TROpospheric chemical composition over the past 40 years project (RETRO) (Schultz
187   et al., 2008) were used for O_3 precursor emissions from biomass burning for the whole land
188   area. RETRO data were available for each year until 2000 in the simulation period, and data
189   for 2000 were used for years after 2000. Historical transition of the atmospheric
190   concentrations of carbon dioxide, nitrous oxide (N_2O), and CH_4 were prescribed with those
191   used in Nozawa et al. (2005), which were somewhat old estimations of the historical
192   evolution in greenhouse gas concentrations, but not much different from recent estimations
193   such as for the Representative Concentration Pathways (RCPs) (Meinshausen et al., 2011).
194   The difference in the concentrations between both estimations were generally within a couple
195   of percent in the simulation period.

196   The linear trends of NO_x and NMVOC annual emissions used in this study in the simulation
197   period of 1980–2005 are shown in Fig. 1. The long-term trends of emissions of both species
198   showed generally similar geographical features to each other; large decrease trends in central
199   Europe, Scandinavia, western Russia, and Kazakhstan, whereas there were widely spread
200   increasing emissions in West, South, Southeast, and East Asia, almost all Africa and Central
201   and South America except for inland Brazil. In North America, NO_x emission generally
202   decreased in the simulation period except for the west coast and New England area of the
203   USA, but that of NMVOC mostly increased with a few patchy exceptions. The trends of NO_x
204   and NMVOC emissions mentioned above were mainly due to the change in anthropogenic
205   emissions, while the change in biomass burning emissions led to a discernible trend in several
206   regions such as inland Brazil and the south of Sahel.

207   The long-term evolution of annual emissions of NO_x and NMVOC over several source areas
208   in the Northern Hemisphere is shown in Fig. 2. Because the emission data were the
209   combination of three different datasets outside Asia, there were somewhat discontinuous
210   changes at the joint years (1990 and 1995) in European and North American emissions. The
211   emissions of NO_x and NMVOC over Europe had peaks around 1990 and generally decreased
212   afterward. Over North America, both species showed small long-term trends: slight decreases
213   in NO_x and slight increases in NMVOC emissions. The emissions of both species over China
214   greatly increased during the whole period. The NO_x emissions were about 4.0 times larger in
215   2005 than 1980 and correspondingly NMVOC was 2.5 times larger, which made emissions of
216   both species for China equal to or even surpassing those for Europe or North America in 2005.
217   The emissions of both species over the Korean Peninsula increased approximately 2.8 times
218   during this period. However, those over Japan showed no such increase: NO_x emission
219   decreased until 1995 and thereafter remained stable, whereas NMVOC emissions went up
220   until 1995 and then slightly decreased.

221   **2.2.2 Tracer tagging**

222   We conducted a 26-year simulation using the full-chemistry setup of CHASER with all the
223   forcings mentioned above, followed by another 26-year simulation with the tracer-transport

Atmospheric
Chemistry
and Physics
Discussions

224   setup of CHASER which calculated the concentration of hypothetical O_3 tracers, each tagged
225   with a particular region in the model domain. The procedure to tag a tracer with each region
226   in the second simulation was the same as used by Nagashima et al. (2010) and a brief
227   description follows. In the second simulation, the transport and dry deposition of each O_3
228   tracer were calculated same as in the first simulation, however the chemical development of
229   tracers was calculated using the chemical production (P) and loss frequencies (L) of the
230   extended odd oxygen family $[O_x = O_3 + O + O(^1D) + NO_2 + 2NO_3 + 3N_2O_5 + PANs + HNO_3$
231   + other nitrates] calculated and archived in the first simulation. In the first simulation, 3D
232   fields of P and L were outputted every 6 hours. Each O_3 tracer could be lost chemically
233   everywhere in the model domain at the frequency of L, but could be chemically produced
234   only inside its tagged region. In the stratosphere over the tropopause defined by the lapse rate,
235   the concentration of O_3 tracer tagged with the stratosphere was assimilated into the same
236   stratospheric O_3 data as used in the first simulation, but the concentration of the tracers tagged
237   with the region in the troposphere were all set to zero. The calculated concentration of each
238   tagged O_3 tracer at a given location represents the contribution of O_3 produced in each source
239   region and transported to that location.

240   The horizontal and vertical separation of the model domain for the tracer tagging was also
241   the same as used by Nagashima et al. (2010). The troposphere in the model domain was
242   horizontally separated into 22 regions and each horizontal region was further separated
243   vertically between the free troposphere (FT) and the planetary boundary layer (PBL). The
244   stratosphere was considered one separate source region, that is, the model domain was
245   separated into 45 source regions. The 22 regions for horizontal separation are shown in Fig. 1
246   and each region was assigned a three-letter code (e.g., AMN for North America) which is
247   used in the following sections. For the vertical separation of the source regions in the
248   troposphere, the PBL was defined as the lowest six layers in the model (surface to about 750
249   hPa), based on the observed and modeled vertical profiles of O_3 production.

250   The long-term tracer-tagging simulation allowed estimation of the long-term variations in
251   contributions of each source region to the O_3 concentration at given receptor locations. This is
252   important information to explain the cause of the reported increasing trend in surface O_3 over
253   East Asia. However, it should be noted that the tracer-tagging simulation calculates the
254   amount of O_3 in a receptor location that was produced chemically in each source region from
255   O_3 precursors emitted both from the source region and adjacent source regions. Thus, the
256   contribution of a source region estimated in tracer-tagging simulation should not be fully
257   attributed to emissions of O_3 precursors in that source region. Emission sensitivity simulation
258   is another method of estimating the portion of O_3 fully attributable to a change in O_3 precursor
259   emissions in a source region, and takes the difference of simulated O_3 between two model
260   runs with and without perturbed O_3 precursor emissions in that source region. The resulting
261   estimations of source contributions by the two methods can differ; however, the differences
262   have not yet been well quantified. Li et al. (2008) reported that the difference between the two
263   methods could be as much as 30 % in source apportionment estimation for one location and
264   time (i.e., Mt. Tai in central eastern China in June 2006). Wang et al. (2011) found somewhat
265   larger differences in the contributions of China to domestic O_3 concentration between the two
266   methods for each month of the year, but no discussions were made for O_3 over Japan.

267   Nevertheless, we employed the tracer-tagging simulation to study the cause of reported long-
268   term change in surface O_3 over Japan mainly due to its computational efficiency. Thus, the
269   results should be carefully interpreted in terms of the difference between the source regions of
270   chemical O_3 production and those of O_3 precursor emissions. The computational efficiency
271   resulting from the tracer-tagging approach and relatively coarse horizontal resolution enabled

272 us to make several sensitivity simulations with the different combination of forcings for long-
273 term simulation. In the following sections, the simulation with the full set of long-term
274 forcings described above, hereinafter referred to as "standard" simulation, is initially analyzed.
275 This is then further interpreted using the results of sensitivity simulations; the specific settings
276 of sensitivity simulations are also described.

277

278 **3   Results and discussion**

279 **3.1   Long-term evolution of surface O_3 over Japan**

280 Nagashima et al. (2010) validated how well CHASER can reproduce the observed features
281 of surface O_3 concentrations by comparing the simulated surface O_3 concentrations with
282 observations taken during 2000–2005 at several sites mainly in rural areas in the Northern
283 Hemisphere, and CHASER successfully simulated the annual variation of surface O_3 in a
284 variety of regions. In this study, the horizontal resolution of the model differed from that used
285 in Nagashima et al. (2010); however, the model well represented the observed concentrations
286 and seasonal evolutions of surface O_3 (Fig. S1 and Table S1 in the Supplement). The surface
287 O_3 over Japan has been observed at ambient air quality monitoring stations since the early
288 1970s when severe air pollution occurred in industrial or urban areas. The monitoring data
289 have been compiled by the Atmospheric Environmental Regional Observation System
290 (AEROS). The number of stations increased since the launch of the system and, for the period
291 of simulation (1980–2005), about 1000 monitoring stations widely distributed throughout
292 Japan except in the southern islands could be used for validation of the model results. The
293 monitoring data of AEROS have been used to examine the long-term variation of surface O_3
294 over Japan in several studies and showed significant increasing trends (Ohara and Sakata,
295 2003; Ohara et al., 2008; Kurokawa et al., 2009; Akimoto et al., 2015). We validated the
296 simulated surface O_3 over Japan with the AEROS data in terms of the long-term variation in
297 the following.

298 For the validation, the monitoring sites selected had continuously observed the surface O_3
299 during the simulation period (1980–2005). To ensure continuity of sites, we selected
300 monitoring sites with annual mean surface O_3 available for every year in the simulation period.
301 The annual mean data at a monitoring site was calculated as the average of monthly means
302 when available for more than 9 months, the monthly mean was calculated from daily means
303 when available for over 19 days per month, and the daily mean was calculated from hourly
304 means when available for more than 19 hours per day. There were 339 sites, located mainly in
305 populated areas of Japan except in the northernmost island (Hokkaido) and southern islands
306 (Nansei Islands). We first calculated the annual mean surface O_3 from the observed hourly
307 data at each monitoring site as described above, and then the annual means of all sites were
308 averaged to calculate the observed annual mean surface O_3 over Japan. The simulated annual
309 mean surface O_3 over Japan was calculated as the average of annual means of the model grids,
310 which included the locations of monitoring sites selected for the validation. Therefore, the
311 model grids including Hokkaido or Nansei Islands were not used to calculate the simulated
312 annual mean. The temporal variations of observed and simulated annual mean surface O_3
313 anomalies during 1980–2005 averaged over Japan are shown in Fig. 3. During the period, the
314 observed annual mean surface O_3 over Japan showed a clear increasing trend with a linear
315 increase of about 2.70 ppbv/decade, which was significant at the 5 % risk level. The simulated
316 annual mean surface O_3 over Japan also showed a significant increasing trend with a rate of
317 about 2.58 ppbv/decade, which corresponded well to the observed increase in surface O_3 over

Atmospheric
Chemistry
and Physics
Discussions

Open Access

EGU

318 Japan. The value of the linear increasing trend and the observed features of IAVs in surface
319 O_3 over Japan – such as a rapid increase from the mid-1980s to the mid-1990s followed by a
320 stagnation of increase for about 7–8 years and a further increase in the past several years –
321 were reasonably well captured by the model.

322 The model also well represented the longitudinal differences in the long-term trend of
323 surface O_3 in Japan. Figure 4 shows the maps of linear trends of annual mean surface O_3
324 during 1980–2005 calculated from the model simulations and observations at AEROS
325 monitoring sites as selected for Fig. 3. The simulated annual mean surface O_3 showed an
326 increasing trend in the whole area including all of Japan and the Korean Peninsula (Fig. 4a).
327 The simulated increasing trend of annual mean surface O_3 well exceeded 2.0 ppbv/decade in
328 wide areas of Japan except for Hokkaido, and tended to be greater toward western Japan,
329 which is nearer to the Asian continent. However, the increasing trends of observed annual
330 mean surface O_3 at each monitoring site (Fig. 4b) differed greatly from each other even in
331 nearby sites, and there was no apparent longitudinal tendency in trends at individual
332 monitoring sites. However, we averaged the observed annual mean surface O_3 at individual
333 monitoring sites at longitudinal intervals (approximately 2.8°) of the model grids as shown by
334 gray rectangles (Fig. 4b) and calculated the long-term trend of averaged monitoring data at
335 each longitudinal band. The calculated increasing trends were clearly larger toward the west,
336 which was consistent with westward rise of the increasing trends of simulated data.

337 There were seasonal differences in the long-term increasing trend of surface O_3 over Japan.
338 The temporal variations of observed and simulated seasonal mean surface O_3 anomalies
339 during 1980–2005 averaged over Japan are shown in Fig. 5. The increasing trend of surface
340 O_3 over Japan in the monitoring data was greatest in spring (March–May: 4.04 ppbv/year) and
341 was also large in summer (June–August: 3.07 ppbv/year); in contrast, increasing trends were
342 relatively small in fall (September–November: 2.29 ppbv/year) and winter (December–
343 February: 1.28 ppbv/year). Seasonal dependency in the increasing trends of observed surface
344 O_3 over Japan has been previously reported (Ohara and Sakata, 2003; Naja and Akimoto,
345 2004; Parrish et al., 2012). Ohara and Sakata (2003) examined almost the same O_3 monitoring
346 data in Japan as used in the present study for the period 1985–1999 and showed year-round
347 increase in surface O_3 from 1985–1987 to 1997–1999 with a greater increase in the warm
348 season (March–August) than in the rest of the year. Naja and Akimoto (2004) also reported a
349 larger increase of O_3 in the warm season between the period 1970–1985 and 1986–2002 in the
350 boundary layer over Japan by analyzing ozonesonde data at four sites. Parrish et al. (2012)
351 summarized long-term changes in lower tropospheric baseline O_3 over the world including
352 two regions in Japan (Mt. Happo and several sites in the marine boundary layer grouped as
353 one region), and showed that the increasing trend of surface O_3 was greatest in spring and
354 least in fall in these two regions. In the present study, the simulated increasing trend in
355 seasonal mean surface O_3 was also larger in the warm (spring–summer) than in the cold
356 season (fall–winter), consistent with the observed increasing trends.

357 As described above, our model captured well the basic features of long-term trends in
358 observed surface O_3 over Japan, which allowed us to use the simulated data for further
359 analysis on the source of the long-term trend in the next section.

360

3.2 Contributions of O_3 production regions

362 The tracer-tagging simulation for 1980–2005 was conducted to examine the long-term
363 variations of O_3 tracers tagged by regions of photochemical production. IAVs in the annual

364   mean concentrations of each tagged O_3 tracer averaged over Japan are shown in Fig. 6. The
365   tagged tracers other than FT and stratosphere in Fig. 6 and the following figures represent the
366   contribution of O_3 produced in the PBL of different source regions shown in Fig. 1, where
367   contributions of several source regions were grouped into some combined source regions. It
368   should be noted that the model grids used for averaging in these figures differed from those in
369   Figs. 3–5. They encompassed almost all of Japan excluding the Nansei Islands in order to
370   examine temporal behavior of tagged O_3 tracers in all of Japan (see Fig. 4 for actual areas for
371   averaging).

372   Domestically created O_3 was the largest contribution to surface O_3 concentration averaged
373   over Japan during the whole simulation period. The contribution of domestic production had a
374   large IAV and was larger in the last decade than previously.

375   The second largest contribution was the O_3 created in the FT as a whole during almost the
376   entire period. For the FT, the northern mid-latitude regions such as North Pacific (NPC),
377   Europe (EUR), North Atlantic (NAT), North America (AMN), and China (CHN) made
378   leading contributions during the period; however, the increasing trend of these contributions
379   was considerable particularly for CHN and NPC (Fig. S2). Despite such differences among
380   the regional contributions in the FT, we hereafter only considered the total of each regional
381   contribution in the FT, since it was difficult to associate a regional contribution with a
382   particular source region of O_3 precursor emissions. The precursors eventually resulted in O_3
383   production in a region in the FT can be transported longer distance due to faster wind speed in
384   the FT and therefore would be influenced by emissions from a wider range of source regions
385   than in the PBL. The total FT contribution showed an increasing trend during the period.

386   The NO_x emission from lightning was an indispensable source of NO_x in the FT. The global
387   annual lightning-NO_x emission in the current simulation was about 3.1 TgN/year averaged
388   over the entire period and showed a small but significant increase of about 0.012 TgN/year
389   (0.39 %/year). The increase in lightning-NO_x emission was a consequence of changes in
390   convection activities due to the change in climate forced into the model during the period
391   (NCEP/NCAR meteorology and HadISST data). However, this increase in lightning-NO_x
392   emission was not the main cause of the increase in the contribution of the total FT – because a
393   sensitivity simulation with all emissions, CH_4 concentration, and stratospheric O_3 fixed at the
394   year 1980 level but with the same temporal evolution in climate showed a quite similar
395   increase in lightning-NO_x emission but no significant increasing trend in the total FT
396   contribution. Therefore, the main cause of the increasing trend in the total FT contribution
397   was likely to be factors other than the increase in lightning-NO_x emission.

398   The contribution of stratospheric O_3 was also large during the entire period, with
399   considerable temporal fluctuations. The large decreases of stratospheric contribution in the
400   early 1980s and 1990s stemmed from the decline of stratospheric O_3 concentration due to the
401   impact of large volcanic eruptions of Mt. El Chichon in 1982 and Mt. Pinatubo in 1991,
402   respectively (Akiyoshi et al., 2009).

403   In the early 1980s, the combined contributions of far remote regions from Japan in the
404   northern mid-latitude (Remote: EUR, NAT, and AMN) made a significant contribution, the
405   fourth largest, to the surface O_3 over Japan and remained at a steady level of contribution
406   during the study period. At the same time, the contribution of CHN significantly increased
407   from the mid-1980s, overtook the contribution of Remote in the early 1990s, and became the
408   largest single regional contribution – excluding the domestic one (i.e., JPN). Moreover, the
409   contributions of O_3 produced in the Korean Peninsula (KOR), the coastal regions in East Asia
410   [E-Asia-Seas: NPC, East China Sea (ECS), and Japan Sea (JPS)], and West-South-SouthEast

Atmospheric
Chemistry
and Physics
Discussions

411 (WSSE) Asian regions [including Middle East (MES), India (IND), Indochina and Philippines
412 (IDC), and Indonesia etc. (IDN)] also showed obvious increasing trends.

413 The linear trend (ppbv/decade) of annual mean tagged O_3 tracers during the simulation
414 period as well as that of the total O_3, which is the sum of all tagged O_3 tracers averaged over
415 whole Japan (JPN-ALL) and those averaged over three sub-regions in Japan: western (JPN-
416 W), eastern (JPN-E), and northern (JPN-N) Japan is shown in Fig. 7 (see Fig. 4 for the
417 definition of sub-regions). The trend was calculated from the annual mean concentrations.
418 The increasing trend of total O_3 averaged over JPN-ALL was 2.37 ppbv/decade, which was
419 somewhat smaller than estimated in Fig. 3 (2.58 ppbv/decade) due to inclusion of model grids
420 in JPN-N for averaging where the simulated increasing trend of O_3 was relatively small. The
421 increasing trend of total O_3 tended to be greater westward. The absolute contribution of
422 domestically produced O_3 in Japan differed among the regions – it tended to be larger in JPN-
423 E than other parts of Japan (Nagashima et al., 2010); however, there were no such regional
424 differences in long-term trends. The westward tendency of larger increasing trends in total O_3
425 over Japan was mainly due to the similar tendency in the trends of the contribution of CHN,
426 KOR, and E-Asia-Seas, which strongly suggested a large impact of intra-regional
427 transboundary air pollution in East Asia. In particular, the increasing trend in the CHN
428 contribution was the largest for all sub-regions in Japan. The increasing trend in the
429 contributions of total FT and WSSE Asia was slightly smaller for JPN-N than for other parts
430 of Japan, which also contributed to the regional differences of the trend in total O_3 over Japan.
431 Interestingly, the contribution of Remote showed a small but significant increase only in JPN-
432 N – although emissions of O_3 precursors, NO_x in particular, in Remote did not increase during
433 the period. Due to the large interannual fluctuation, the linear long-term trend of the
434 stratospheric contribution was non-significant for all regions in Japan.

435 The linear trend of tagged O_3 tracers and total O_3 averaged over all of Japan in spring,
436 summer, fall, and winter is shown in Fig. 8. The increasing trends of total O_3 in decreasing
437 order were spring, summer, winter, and fall. This is quite consistent with the seasonal
438 differences in the increasing trend of O_3 observed at several Japanese sites from the 1990s to
439 2011 (Parrish et al., 2012). The increasing trend in the CHN contribution was the largest of all
440 contributions in all four seasons and the trend was particularly large in spring. The KOR
441 contribution was also larger in spring than in other seasons, with the trend in summer of low
442 statistical significance due to relatively large IAVs. The contribution of E-Asia-Seas increased
443 significantly in all seasons. Seasonal differences in the increasing trend in the E-Asia-Seas
444 contribution were small, but were slightly larger in the warm (spring–summer) than the cold
445 season (fall–winter). The increasing trend in domestic (JPN) contribution was larger in spring
446 than in summer similarly to the cases of CHN and KOR contributions, but trends in both
447 seasons were non-significant; whereas those in the cold season were significantly larger than
448 in the warm season. The FT and WSSE Asian contributions showed semi-annual change in
449 their increasing trends; larger in summer and winter than in spring and fall. The contribution
450 of Remote showed a significant increasing trend only in winter; conversely that of Central-
451 North (CN) Asian regions [Central Asia (CAS) and East Siberia (ESB)] showed small but
452 significant decreasing trends in the cold season but non-significant trends in the warm season.
453 The seasonal features in each regional contribution described above enabled explanation of
454 the cause of the seasonality of increasing trend in total O_3 over Japan as follows. The largest
455 increasing trend of total O_3 in spring was predominantly attributed to the large increasing
456 trend in contributions of source regions in northeast Asia (CHN, KOR, E-Asia-Seas, and JPN).
457 The increasing trends in the contributions of CHN, KOR, and JPN were smaller in summer,
458 however, partly compensated by the growth of increasing trends in the FT and WSSE Asian

Atmospheric
Chemistry
and Physics
Discussions

459   contributions from spring to summer. In the cold season, trends for most regions were smaller
460   than in the warm season, except for JPN. The increasing trend in contributions of northeast
461   Asian regions differed little between fall and winter; however, those of FT, WSSE Asia, and
462   Remote had larger increasing trends in winter than in fall, which made the increasing trend of
463   total O_3 in winter larger than in fall.

464   Table 1 summarizes the linear trends of annual mean tagged O_3 tracers and the total O_3
465   averaged over JPN-ALL. The vast majority (about 97 %) of the trend in total O_3 was balanced
466   with the sum of those trends in regional contributions with statistical significance. The largest
467   contribution was from the increase of O_3 produced in CHN (0.85 ppbv/decade), which
468   corresponded to about 36 % of the increasing trend of total O_3. The increasing trend in the
469   contribution of the total FT was also large (0.37 ppbv/decade), representing about 16 % of the
470   total O_3 trend. The contributions of northeast Asian regions other than CHN also increased
471   significantly (0.34, 0.29, and 0.27 ppbv/decade for KOR, E-Asia-Seas, and JPN, respectively)
472   and each accounted for about 12–15 % of the total O_3 trend. About 7 % of the total O_3 trend
473   was attributable to the increasing trend in WSSE Asian contributions (0.16 ppbv/decade). The
474   linear trends in the contributions of remaining regions [CN Asia, Remote, stratosphere, and
475   the others (OTH)] were small and non-significant, and so were not important concerning the
476   cause of reported surface O_3 increase over Japan.

477

3.3   Impact of IAVs in O_3 precursor emissions in different source regions on regional O_3 production

480   The results in the preceding section revealed the relative importance of O_3 produced in
481   different regions to the recent increasing trend in surface O_3 over Japan. It is noteworthy that
482   this does not indicate the relative importance of the different regions of O_3 precursor
483   emissions. For example, there were significant contributions of E-Asia-Seas to the increasing
484   trend in surface O_3 over Japan, but there were clearly no large emission sources of precursors
485   in these maritime regions other than navigation. The increasing trend in the contribution of E-
486   Asia-Seas was likely a consequence of increased transport of O_3 precursors to this region,
487   which had been emitted in adjacent land areas. However, the tracer-tagging approach cannot
488   distinguish the differences in origins of emissions of precursors that resulted in O_3 production
489   in E-Asia-Seas. To further investigate the roles of different regions in the recent increasing
490   trend of surface O_3 over Japan, we performed a series of sensitivity simulations with different
491   assumptions for the temporal variation of factors, which would affect the surface O_3 over
492   Japan. Each sensitivity simulation consisted of a 26-year simulation with full-chemistry setup
493   of CHASER followed by another 26-year simulation with tracer-tagging setup of CHASER.
494   Initially, a sensitivity simulation was performed that was only forced by the IAVs in the
495   climate (NCEP/NCAR meteorology and HadISST data) but with all emissions of O_3
496   precursors, CH_4 concentration, and stratospheric O_3 fixed at the year 1980 level; then we
497   gradually added the increase or the IAV of chemical factors as summarized in Table 2. The
498   simulation F, driven by the IAV of all forcings, was identical to the standard simulation; and
499   simulation A was mentioned concerning lightning-NO_x emission in the preceding section
500   (3.2).

501   The linear trends of annual mean total O_3 and tagged O_3 tracers that had significant effects
502   on the standard simulation averaged over all of Japan in all simulations are shown and
503   compared in Fig. 9. Simulation A showed no obvious increasing trend in total O_3 over Japan.

Atmospheric
Chemistry
and Physics
Discussions

504   The JPN and total FT contributions exhibited increasing trends (0.12 and 0.06 ppbv/decade,
505   respectively), likely due to the IAV of the climate, but they were non-significant.

506   The increase in atmospheric concentration of CH_4 was added in simulation B, because this
507   would have a non-negligible impact on tropospheric O_3 (background O_3 in particular), as
508   frequently reported (Brasseur et al., 2006; Kawase et al., 2011; HTAP, 2010 and references
509   therein). In the simulations other than A, we used a CH_4 concentration increase rate of about
510   12.3 ppbv/year (0.73 %/year) during 1980–2000 and flattened thereafter. In simulation B, the
511   contribution of the total FT showed a significant increasing trend (0.18 ppbv/decade) as did
512   that of Remote (0.08 ppbv/decade; data not shown). The contributions of several other regions
513   such as CHN, E-Asia-Seas, and WSSE Asia also showed slight increasing trends
514   (approximately 0.01–0.02 ppbv/decade), although non-significant. Note that these values
515   included the impact of CH_4 increase as well as the IAV of the climate and, consequently, the
516   total O_3 in simulation B showed a significant increasing trend of about 0.44 ppbv/decade,
517   representing about 19 % of the increasing trend in total O_3 in the standard simulation (2.37
518   ppbv/decade).

519   In simulations C–E, the IAVs in emission of O_3 precursors in northeast Asian regions were
520   gradually added: CHN, KOR, and JPN, respectively. The increase in emissions of O_3
521   precursors in CHN in simulation C caused a large significant increasing trend in the
522   contribution of CHN itself (0.83 ppbv/decade). Moreover, the emission increase in CHN also
523   had a large impact on the contributions of other regions, in particular, the increase trends in
524   the contributions of KOR and E-Asia-Seas became significant: 0.12 and 0.15 ppbv/decade,
525   respectively. The JPN and the total FT contributions also showed somewhat larger increasing
526   trends in simulation C than in B, but the growth in trends between the two simulations was
527   not as large as those of KOR and E-Asia-Seas. The total effect of the emission increase in
528   CHN on the increasing trend in surface O_3 over Japan, assessed using the difference in total
529   O_3 trend between simulations B and C, was about 1.08 ppbv/decade and corresponded to
530   about 46 % of the increasing trend in total O_3 in the standard simulation. The relative
531   contribution of CHN as a source region of O_3 production to the surface O_3 increasing trend
532   over Japan was estimated as 36 % in the preceding section (3.2); however, the contribution of
533   CHN as a source region of O_3 precursors emission was somewhat (10 %) larger due to the
534   production of O_3 outside CHN. It is noteworthy that the slight increasing trend in the
535   contribution of WSSE Asia shown in the CH_4 increase in simulation B was smaller in
536   simulation C. The contributions of Remote and the stratosphere showed similar responses.
537   The increase in O_3 precursor emissions in CHN seemed to partly offset the increase in
538   influence of long range transport of O_3 from such regions.

539   The increase in emissions from KOR in addition to CHN in simulation D gave rise to a
540   much larger increasing trend in the contributions of KOR itself (0.38 ppbv/decade).
541   Compared with simulation C (0.12 ppbv/decade), about one-third of the increasing trend in
542   the contribution of KOR was attributed to the O_3 precursor emission increase in CHN and the
543   rest to emission increase in KOR. Similarly, the emission increase in KOR caused a larger
544   increasing trend in the contributions of E-Asia-Seas in simulation D (0.25 ppbv/decade). We
545   attributed about half of the increasing trend in the contribution of E-Asia-Seas in the standard
546   simulation (0.29 ppbv/decade) to the impact of O_3 precursor emission increase in CHN (and
547   partly that of the CH_4 increase: 0.15 ppbv/decade) as shown in simulation C, about one-third
548   to that in KOR, and the rest to that in regions other than northeast Asia. By further adding the
549   IAV in the domestic (JPN) emissions in simulation E, the increasing trend in the domestic
550   contribution became significant (0.28 ppbv/decade), implying that the increasing trend in
551   domestically produced O_3 was from a combination of multiple factors each of which did not

Atmospheric
Chemistry
and Physics
Discussions

552   cause a significant increase. The total effect of the emission increase in KOR on the
553   increasing trend in surface O_3 over Japan assessed as the difference between simulations C
554   and D was about 0.38 ppbv/decade; and that of the IAV of domestic emission in Japan
555   assessed as the difference between simulations D and E was about 0.09 ppbv/decade; each of
556   which corresponded to about 16 and 4 % of the increasing trend in total O_3 in the standard
557   simulation, respectively.

558   The IAV in emissions of O_3 precursors in northeast Asian regions (CHN, KOR, and JPN)
559   together with the IAV in the climate and the increase in CH_4 concentration induced a
560   significant increasing trend in total O_3 over Japan with a rate of 1.99 ppbv/decade. This
561   accounted for about 84 % of the increasing trend in total O_3 in the standard simulation. The
562   rest of the increasing trend should be regarded as from O_3 precursor emission changes in
563   regions other than northeast Asia. The difference between simulations E and F (standard
564   simulation) showed that the emission change in such regions influenced surface O_3 over Japan
565   mainly through increasing the O_3 production in WSSE Asia and the FT (Fig. 9).

566

4   Summary and conclusion

568   We demonstrated the relative importance of the regions of photochemical O_3 production in
569   the global atmosphere on the long-term increasing trend in surface O_3 over Japan reported in
570   recent decades by conducting a series of tracer-tagging simulations using the global CTM
571   CHASER. The impact of the IAVs of climate, of CH_4 concentration, and of emission of O_3
572   precursors (NO_x and NMVOC) in different source regions on regional photochemical O_3
573   production were also investigated.

574   The observed increasing trend of surface O_3 over Japan for 1980–2005 (2.70 ppbv/decade
575   for annual mean over whole Japan) was successfully reproduced by the model (2.58
576   ppbv/decade) including an obvious tendency of increase toward western Japan and to be
577   greater in the warm (spring–summer) than in the cold season (fall–winter).

578   The absolute contribution of each photochemical O_3 production region to the surface O_3 over
579   Japan represented by the concentrations of tagged O_3 tracer showed different temporal
580   evolution by regions. The contributions of all Asian regions except the northern part (i.e.,
581   CHN, KOR, E-Asia-Seas, JPN, and WSSE) as well as those of the total FT exhibited
582   significant increasing trends during the period. The increasing trend in the contribution of
583   domestically produced O_3 in Japan (i.e., JPN) did not differ much among the different regions
584   in Japan. However, there was a tendency in the increasing trends in contributions of CHN,
585   KOR, and E-Asia-Seas to be large toward western Japan, which was a main cause of the same
586   tendency in the increasing trend in total O_3 and suggested a large impact of intra-regional
587   transboundary air pollution in East Asia.

588   The trends in contributions of most O_3 production regions, except JPN, were larger in the
589   warm than in the cold season, providing a basis for the seasonality in the increasing trend in
590   total O_3 over Japan. Thus, the larger increasing trend of total O_3 in spring than in summer was
591   mainly due to the same tendency in increasing trends in the contributions of northeast Asian
592   regions (CHN, KOR, and JPN), although this was partly compensated by larger increasing
593   trends in the FT and WSSE Asia contributions in summer than spring. In the cold season, the
594   contributions of FT, WSSE Asia, and Remote had larger increasing trends in winter than in
595   fall, which led to a larger increasing trend in total O_3 in winter than in fall.

596   The sum of the trends in contributions of O_3 production regions with sufficient statistical
597   significance accounted for most (about 97 %) of the increasing trend in total O_3 over Japan

13

598 (2.37 ppbv/decade). The largest portion was attributed to the increasing trend of O_3 produced
599 in CHN (36 %; 0.85 ppbv/decade), followed by that in the total FT (16 %; 0.37 ppbv/decade).
600 The increasing trend in contributions of the other northeast Asian regions (KOR, E-Asia-Seas,
601 and JPN; 0.27–0.34 ppbv/decade) each accounted for about 12–15 % of the total O_3 trend, and
602 the majority of the rest of the total O_3 trend (7 %; 0.16 ppbv/decade) was attributable to
603 WSSE Asia.

604   We further investigated the impact of the IAV of controlling factors, such as climate, CH_4
605 concentration, and emission of O_3 precursors, on photochemical O_3 production in different
606 source regions and its influence on the long-term increasing trend in surface O_3 over Japan
607 through a series of sensitivity simulations that gradually added the IAV of these factors. The
608 IAV of the climate and the increase in CH_4 concentration together caused the increase of
609 photochemical O_3 production in several regions and resulted in the significant increasing
610 trend in surface O_3 over Japan (0.44 ppbv/decade) and represented about 19 % of the
611 increasing trend in surface O_3 in the standard simulation. The increase in emission of O_3
612 precursors in CHN led to the increase of photochemical O_3 production in northeast Asian
613 regions including CHN itself, KOR, JPN, and E-Asia-Seas; and the resulting increasing trend
614 in surface O_3 over Japan (1.08 ppbv/decade) accounted for about 46 % of that in the standard
615 simulation. The relative contribution of CHN to the surface O_3 increasing trend over Japan as
616 the source region of O_3 precursor "emission" was 10 % larger than as the source region of O_3
617 "production" due to production of O_3 outside of CHN. Then, the impact of the O_3 precursor
618 emission change in KOR and JPN on the increasing trend in surface O_3 over Japan (about
619 0.38 and 0.10 ppbv/decade, respectively) corresponded to 16 and 4 % of the increasing trend
620 in total O_3 in the standard simulation, respectively. The rest of the increasing trend in total O_3
621 in the standard simulation (about 16 %) was attributed to O_3 precursor emission change in
622 regions other than northeast Asia, mainly through increasing the photochemical O_3 production
623 in WSSE Asia and the total FT.

624

632

Atmospheric
Chemistry
and Physics
Discussions

633 **References**

634 Akimoto, H., Mori, Y., Sasaki, K., Nakanishi, H., Ohizumi, T., and Itano, Y.: Analysis of
635   monitoring data of ground-level ozone in Japan for longterm trend during 1990–2010:
636   Causes of temporal and spatial variation, Atmos. Environ., 102, 302–310, 2015.

637 Akiyoshi, H., Zhou, L. B., Yamashita, Y., Sakamoto, K., Yoshiki, M., Nagashima, T.,
638   Takahashi, T., Kurokawa, J., Takigawa, M., and T. Imamura, T.: A CCM simulation of the
639   breakup of the Antarctic polar vortex in the years 1980–2004 under the CCMVal scenarios,
640   J. Geophys. Res., 114, D03103, doi:10.1029/2007JD009261, 2009.

641 Brasseur, G. P., Schultz, M., Granier, C., Saunois, M., Diehl, T., Botzet, M., and Roeckner,
642   E.: Impact of climate change on the future chemical composition of the global troposphere,
643   J. Clim., 19, 3932–3951, doi:10.1175/JCLI3832.1, 2006.

644 Chang, S.-C. and Lee, C.-T.: Evaluation of the trend of air quality in Taipei, Taiwan from
645   1994 to 2003, Environ. Monit. Assess., 127, 87–96, doi:10.1007/s10661-006-9262-1, 2007.

646 Chou, C. C.-K., Liu, S. C., Lin, C.-Y., Shiu, C.-J., and Chang, K.-H.: The trend of surface
647   ozone in Taipei, Taiwan, and its causes: Implications for ozone control strategies, Atmos.
648   Environ., 40, 3898–3908, 2006.

649 Cooper, O. R., Parrish, D. D., Ziemke, J., Balashov, N. V., Cupeiro, M., Galbally, I. E., Gilge,
650   S., Horowitz, L., Jensen, N. R., Lamarque, J.-F., Naik, V., Oltmans, S. J., Schwab, J.,
651   Shindell, D. T., Thompson, A. M., Thouret, V., Wang, Y., and Zbinden, R. M.: Global
652   distribution and trends of tropospheric ozone: An observation-based review, Elementa, 2,
653   000029, doi: 10.12952/journal.elementa.000029, 2014.

654 Ding, A. J., Wang, T., Thouret, V., Cammas, J.-P., and Nédélec, P.: Tropospheric ozone
655   climatology over Beijing: analysis of aircraft data from the MOZAIC program, Atmos.
656   Chem. Phys., 8, 1–13, 2008.

657 Eyring, V., Harris, N. R P., Rex, M., Shepherd, T. G., Fahey, D. W., Amanatidis, G. T.,
658   Austin, J., Chipperfield, M. P., Dameris, M., Forster, P. M. De F., Gettelman, A., Graf, H.
659   F., Nagashima, T., Newman, P. A., Pawson, S., Prather, M. J., Pyle, J. A., Salawitch, R. J.,
660   Santer, B. D., and Waugh, D. W.: A strategy for process-oriented validation of coupled
661   chemistry-climate models. Bull. Am. Meteorol. Soc., 86, 1117–1133, 2005.

Atmospheric
Chemistry
and Physics
Discussions

662   HTAP, UNECE: Hemispheric Transport of Air Pollution 2010: Part A: Ozone and Particulate
663   Matter, Air Pollution Studies No. 17, (ed. by Dentener, F., Keating, T., and Akimoto, H.),
664   ECE/EN.Air/100, 2010.

665   Kalnay, E., Kanamitsu, M., Kistler, R., Collins, W., Deaven, D., Gandin, L., Iredell, M., Saha,
666   S., White, G., Woollen, J., Zhu, Y., Leetmaa, A., Reynolds, B., Chelliah, M., Ebisuzaki,
667   W., Higgins, W., Janowiak, J., Mo, K. C., Ropelewski, C., Wang, J., Jenne, R., and Joseph,
668   D.: The NCEP/NCAR 40-year reanalysis project, Bull. Amer. Meteor. Soc., 77, 437–470,
669   1996.

670   Kawase, H., Nagashima, T., Sudo, K., and Nozawa, T.: Future changes in tropospheric ozone
671   under Representative Concentration Pathways (RCPs), Geophys. Res. Lett., 38, L05801,
672   doi:10.1029/2010GL046402, 2011.

673   Kurokawa, J., Ohara, T., Uno, I., Hayasaki, M., and Tanimoto, H.: Influence of
674   meteorological variability on interannual variations of springtime boundary layer ozone
675   over Japan during 1981–2005, Atmos. Chem. Phys., 9, 6287–6304, 2009.

676   Kurokawa, J., Ohara, T., Morikawa, T., Hanayama, S., Janssens-Maenhout, G., Fukui, T.,
677   Kawashima, K., and Akimoto, H.: Emissions of air pollutants and greenhouse gases over
678   Asian regions during 2000–2008: Regional Emission inventory in ASia (REAS) version 2,
679   Atmos. Chem. Phys., 13, 11019–11058, 2013.

680   Lee, H.-J., Kim, S.-W., Brioude, J., Cooper, O. R., Frost, G. J., Kim, C.-H., Park, R. J.,
681   Trainer, M., and Woo J.-H.: Transport of NOx in East Asia identified by satellite and in
682   situ measurements and Lagrangian particle dispersion model simulations, J. Geophys. Res.
683   Atmos., 119, 2574–2596, doi:10.1002/2013JD021185, 2014.

684   Li, J., Wang, Z. F., Akimoto, H., Yamaji, K., Takigawa, M., Pochanart, P., Liu, Y., Tanimoto,
685   H., and Kanaya, Y.: Near-ground ozone source attributions and outflow in central eastern
686   China during MTX2006, Atmos. Chem. Phys., 8, 7335–7351, 2008.

687   Li, H. C., Chen, K. S., Huang, C. H., and Wang, H. K.: Meteorologically adjusted long-term
688   trend of ground-level ozone concentrations in Kaohsiung County, southern Taiwan, Atmos.
689   Environ., 44, 3605–3608, 2010.

690   Lin, S.-J. and Rood, R. B.: Multidimensional flux-form semi-Lagrangian transport scheme,
691   Mon. Weather Rev., 124, 2046–2070, 1996.

Atmospheric
Chemistry
and Physics
Discussions

Open Access

EGU

692 Lin, Y.-K., Lin, T.-H., and Chang, S.-C.: The changes in different ozone metrics and their
693   implications following precursor reductions over northern Taiwan from 1994 to 2007,
694   Environ. Monit. Assess., 169, 143–157, 2010.

695 Logan, J. A., Megretskaia, I. A., Miller, A. J., Tiao, G. C., Choi, D., Zhang, L., Stolarski, R.
696   S., Labow, G. J., Hollandsworth, S. M., Bodeker, G. E., Claude, H., de Muer, D., Kerr, J.
697   B., Tarasick, D. W., Oltmans, S. J., Johnson, B., Schmidlin, F., Staehelin, J., Viatte, P., and
698   Uchino, O.: Trends in the vertical distribution of ozone: A comparison of two analyses of
699   ozonesonde data, J. Geophys. Res., 104, 26373–26399, 1999.

700 Lu, W.-Z. and Wang, X.-K.: Evolving trend and self-similarity of ozone pollution in central
701   Hong Kong ambient during 1984–2002, Sci. Total Environ., 357, 160–168, 2006.

702 Mauzerall, D. L., Sultan, B., Kim, N., and Bradford, D. F.: NOx emissions from large point
703   sources: variability in ozone production, resulting health damages and economic costs,
704   Atmos. Environ., 39, 2851–2866, 2005.

705 Meinshausen, M., Smith. S. J., Calvin, K., Daniel, J. S., Kainuma, M. L. T., Lamarque, J-F.,
706   Matsumoto, K., Montzka, S. A., Raper, S. C. B., Riahi, K., Thomson, A., Velders, G. J. M.,
707   and van Vuuren, D. P. P.: The RCP greenhouse gas concentrations and their extensions
708   from 1765 to 2300, Climatic Change, 109, 213–241, 2011.

709 MOE (Ministry of Environment) Japan: FY 2013 status of air pollution, available online at:
710   http://www.env.go.jp/air/osen/jokyoh25/ (in Japanese), 2013.

711 Nagashima, T., Ohara, T., Sudo, K., and Akimoto, H.: The relative importance of various
712   source regions on East Asian surface ozone, Atmos. Chem. Phys., 10, 11305–11322, 2010.

713 Naja, M. and Akimoto, H.: Contribution of regional pollution and long-range transport to the
714   Asia-Pacific region: Analysis of long-term ozonesonde data over Japan, J. Geophys. Res.,
715   109, D21306, doi:10.1029/2004JD004687, 2004.

716 Nozawa, T., Nagashima, T., Shiogama, H., and Crooks, S. A.: Detecting natural influence on
717   surface air temperature change in the early twentieth century, Geophys. Res. Lett., 32,
718   L20719, doi:10.1029/2005GL023540, 2005.

719 Ohara, T. and Sakata, T.: Long-term variation of photochemical oxidants over Japan, J. Jpn.
720   Soc. Atmos. Environ., 38, 47–54. (in Japanese with English summary), 2003.

Atmospheric
Chemistry
and Physics
Discussions

721   Ohara, T., Yamaji, K., Uno, I., Tanimoto, H., Sugata, S., Nagashima, T., Kurokawa, J., Horii,
722   N., and Akimoto, H.: Long-term simulations of surface ozone in East Asia during 1980–
723   2020 with CMAQ and REAS inventory, In Air Pollution Modelling and Its Application
724   XIX (NATO Science for Peace and Security Series C: Environmental Security) (ed. by
725   Borrego, C., and Miranda, A. I.). Springer, Dordrecht, The Netherlands, 136–144, 2008.

726   Ohara, T., Akimoto, H., Kurokawa, J., Horii, N., Yamaji, K., Yan, X., and Hayasaka, T.: An
727   Asian emission inventory of anthropogenic emission sources for the period 1980–2002,
728   Atmos. Chem. Phys., 7, 4410–4444, 2007.

729   Olivier, J. G. J. and Berdowski, J. J. M.: Global emissions sources and sinks, in: The Climate
730   System, Berdowski, J., Guicherit, R., and Heij, B. J. (eds.), A. A. Balkema Publishers/
731   Swets & Zeitlinger Publishers, Lisse, The Netherlands, 33–78, 2001.

732   Oltmans, S. J., Lefohn, A. S., Harris, J. M., Galbally, I., Scheel, H. E., Bodeker, G., Brunke,
733   E., Claude, H., Tarasick, D., Johnson, B. J., Simmonds, P., Shadwick, D., Anlauf, K.,
734   Hayden, K., Schmidlin, F., Fujimoto, T., Akagi, K., Meyer, C., Nichol, S., Davies, J.,
735   Redondas, A., and Cuevas, E.: Long-term changes in tropospheric ozone, Atmos. Environ.,
736   40, 3156–3173, 2006.

737   Oltmans, S. J., Lefohn, A. S., Shadwick, D., Harris, J. M., Scheel, H. E., Galbally, I., Tarasick,
738   D. W., Johnson, B. J., Brunke, E.-G., Claude, H., Zeng, G., Nichol, S., Schmidlin, F.,
739   Davies, J., Cuevas, E., Redondas, A., Naoe, H., Nakano, T., and Kawasato, T.: Recent
740   tropospheric ozone changes – A pattern dominated by slow or no growth, Atmos. Environ.,
741   67, 331–351, 2013.

742   Parrish, D. D., Law, K. S., Staehelin. J., Derwent, R., Cooper, O. R., Tanimoto, H., Volz-
743   Thomas, A., Gilge, S., Scheel, H.-E., Steinbacher, M., and Chan, E.: Long-term changes in
744   lower tropospheric baseline ozone concentrations at northern mid-latitudes, Atmos. Chem.
745   Phys., 12, 11485–11504, 2012.

746   Rayner, N. A., Parker, D. E., Horton, E. B., Folland, C. K., Alexander, L. V., Rowell, D. P.,
747   Kent, E. C., and Kaplan, A.: Global analyses of sea surface temperature, sea ice, and night
748   marine air temperature since the late nineteenth century, J. Geophys. Res., 108, 4407,
749   doi:10.1029/2002JD002670, 2003.

750   Schultz, M. G., Heil, A., Hoelzemann, J. J., Spessa, A., Thonicke, K., Goldammer, J. G., Held,
751   A. C., Pereira, J. M. C., and van het Bolscher, M.: Global wildland fire emissions from

752   1960 to 2000, Global Biogeochem. Cycles, 22, GB2002, doi:10.1029/2007GB003031,

753   2008.

754   Seo, J., Youn, D., Kim, J. Y., and Lee, H.: Extensive spatiotemporal analyses of surface

755   ozone and related meteorological variables in South Korea for the period 1999–2010,

756   Atmos. Chem. Phys., 14, 6395–6415, 2014.

757   Shindell, D., Kuylenstierna, J. C. I., Faluvegi, G., Milly, G., Emberson, L., Hicks, K., Vignati,

758   E., Van Dingenen, R., Janssens-Maenhout, G., Raes, F., Pozzoli, L., Amann, M., Klimont,

759   Z., Kupiainen, K., Höglund-Isaksson, L., Anenberg, S. C., Muller, N., Schwartz, J., Streets,

760   D., Ramanathan, V., Oanh, N. T. K., Williams, M., Demkine, V., and Fowler, D.:

761   Simultaneously mitigating near-term climate change and improving human health and food

762   security, Science, 335, 183–189, 2012.

763   Silva, R. A., West, J. J., Zhang, Y., Anenberg, S. C., Lamarque, J.-F., Shindell, D. T., Collins,

764   W. J., Dalsoren, S., Faluvegi, G., Folberth, G., Horowitz, L. W., Nagashima, T., Naik, V.,

765   Rumbold, S., Skeie, F., Sudo, K., Takemura, T., Bergmann, D., Cameron-Smith, P., Cionni,

766   I., Doherty, R. M., Eyring, V., Josse, B., MacKenzie, I. A., Plummer, D., Righi, M.,

767   Stevenson, D. S., Strode S., Szopa, S., and Zeng, G.: Global premature mortality due to

768   anthropogenic outdoor air pollution and the contribution of past climate change, Environ.

769   Res. Lett., 8, 034005, 2013.

770   Sudo, K. and Akimoto, H.: Global source attribution of tropospheric ozone: Long-range

771   transport from various source regions, J. Geophys. Res., 112, D12302,

772   doi:10.1029/2006JD007992, 2007.

773   Sudo, K., Takahashi, M., Kurokawa, J., and Akimoto, H.: CHASER: A global chemical

774   model of the troposphere: 1. Model description, J. Geophys. Res., 107(D17), 4339,

775   doi:10.1029/2001JD001113, 2002.

776   Susaya, J., Kim, K.-H., Shon, Z.-H., and Brown, R. J. C.: Demonstration of long-term

777   increases in tropospheric O_3 levels: Causes and potential impacts, Chemosphere, 92, 1520–

778   1528, 2013.

779   Tanimoto, H.: Increase in springtime tropospheric ozone at a mountainous site in Japan for

780   the period 1998–2006, Atmos. Environ., 43, 1358–1363, 2009.

Atmospheric
Chemistry
and Physics
Discussions

Open Access

EGU

781   Tanimoto, H., Ohara, T., and Uno, I.: Asian anthropogenic emissions and decadal trends in
782   springtime tropospheric ozone over Japan: 1998–2007, Geophys. Res. Lett., 36, L23802,
783   doi:10.1029/2009GL041382, 2009.

784   UNEP (United Nations Environment Programme) and WMO (World Meteorological
785   Organization): Integrated Assessment of Black Carbon and Tropospheric Ozone: Summary
786   for   Decision   Makers,   available   online   at
787   http://www.unep.org/dewa/Portals/67/pdf/Black_Carbon.pdf, 2011.

788   US EPA (U.S. Environmental Protection Agency): Air Quality Criteria for Ozone and Related
789   Photochemical Oxidants (Final), U.S. Environmental Protection Agency, Washington, DC,
790   EPA/600/R-05/004aF-cF, 2006.

791   Van Aardenne, J. A., Dentener, F. J., Olivier, J. G. J., Klein Goldewijk, C. G. M., and
792   Lelieveld, J.: A 1 x 1 degree resolution dataset of historical anthropogenic trace gas
793   emissions for the period 1890–1990, Global Biogeochem. Cy., 15(4), 909–928, 2001.

794   Van Leer, B.: Toward the ultimate conservative difference scheme. IV: A new approach to
795   numerical convection, J. Comput. Phys., 23, 276–299, 1977.

796   Wakamatsu, S., Morikawa, T., and Ito, A.: Air Pollution Trends in Japan between 1970 and
797   2012 and Impact of Urban Air Pollution Countermeasures, Asian J. Atmos. Env., 7(4),
798   177–190, 2013.

799   Wang, X. and Mauzerall, D. L.: Characterizing distributions of surface ozone and its impact
800   on grain production in China, Japan and South Korea: 1990 and 2020, Atmos. Environ., 38,
801   4383–4402, 2004.

802   Wang, T., Wei, X. L., Ding, A. J., Poon, C. N., Lam, K. S., Li, Y. S., Chan, L. Y., and Anson,
803   M.: Increasing surface ozone concentrations in the background atmosphere of Southern
804   China, 1994–2007, Atmos. Chem. Phys., 9, 6217–6227, 2009.

805   Wang, Y., Zhang, Y., Hao, J., and Luo, M.: Seasonal and spatial variability of surface ozone
806   over China: contributions from background and domestic pollution, Atmos. Chem. Phys.,
807   11, 3511–3525, 2011.

808   Xu, X., Lin, W., Wang, T., Yan, P., Tang, J., Meng, Z., and Wang, Y.: Long-term trend of
809   surface ozone at a regional background station in eastern China 1991–2006: enhanced
810   variability, Atmos. Chem. Phys., 8, 2595–2607, 2008.

811   Zhang, Q., Yuan, B., Shao, M., Wang, X., Lu, S., Lu, K., Wang, M., Chen, L., Chang, C.-C.,

812   and Liu, S. C.: Variations of ground-level O_3 and its precursors in Beijing in summertime

813   between 2005 and 2011, Atmos. Chem. Phys., 14, 6089–6101, 2014.

814

Atmospheric
Chemistry
and Physics
Discussions

Open Access

815 **Table 1.** Summary of the linear trends of annual mean tagged O_3 tracers as well as the total O_3

816 averaged over Japan (JPN-ALL) for 1980–2005. Bold figures denote that trends are

817 significant at 5 % risk level.

Source Region	Trend [ppbv/dec]	Percent
CHN	**0.85 ± 0.2**	35.8
KOR	**0.34 ± 0.14**	14.6
JPN	**0.27 ± 0.19**	11.5
E-Asia-Seas	**0.29 ± 0.05**	12.4
WSSE Asia	**0.16 ± 0.04**	6.8
N Asia	-0.05 ± 0.08	-2.1
Remote	0.04 ± 0.08	1.7
OTH	0.01 ± 0.02	0.5
FT	**0.37 ± 0.1**	15.5
Strat.	0.08 ± 0.28	3.3
Total	**2.37 ± 0.42**	100.0

818

819

Atmospheric
Chemistry
and Physics
Discussions

Open Access

820   **Table 2.** Summary of the sensitivity simulations and the standard simulation

Simulation code	CH_4 concentration	O₃ precursor emissions				Stratospheric O₃ trend
		CHN	KOR	JPN	ROW[a]	
A	1980[b]	1980	1980	1980	1980	1980
B	increase[c]	1980	1980	1980	1980	1980
C	increase	IAV[d]	1980	1980	1980	1980
D	increase	IAV	IAV	1980	1980	1980
E	increase	IAV	IAV	IAV	1980	1980
F (standard)	increase	IAV	IAV	IAV	IAV	IAV

821   a Precursor emissions in the Rest Of the World (ROW) other than CHN, KOR, and JPN

822   b Each factor was fixed at the year 1980 level

823   c CH_4 concentration increased until 2000 and flattened thereafter

824   d InterAnnual Variation (IAV) of each factor was considered

825
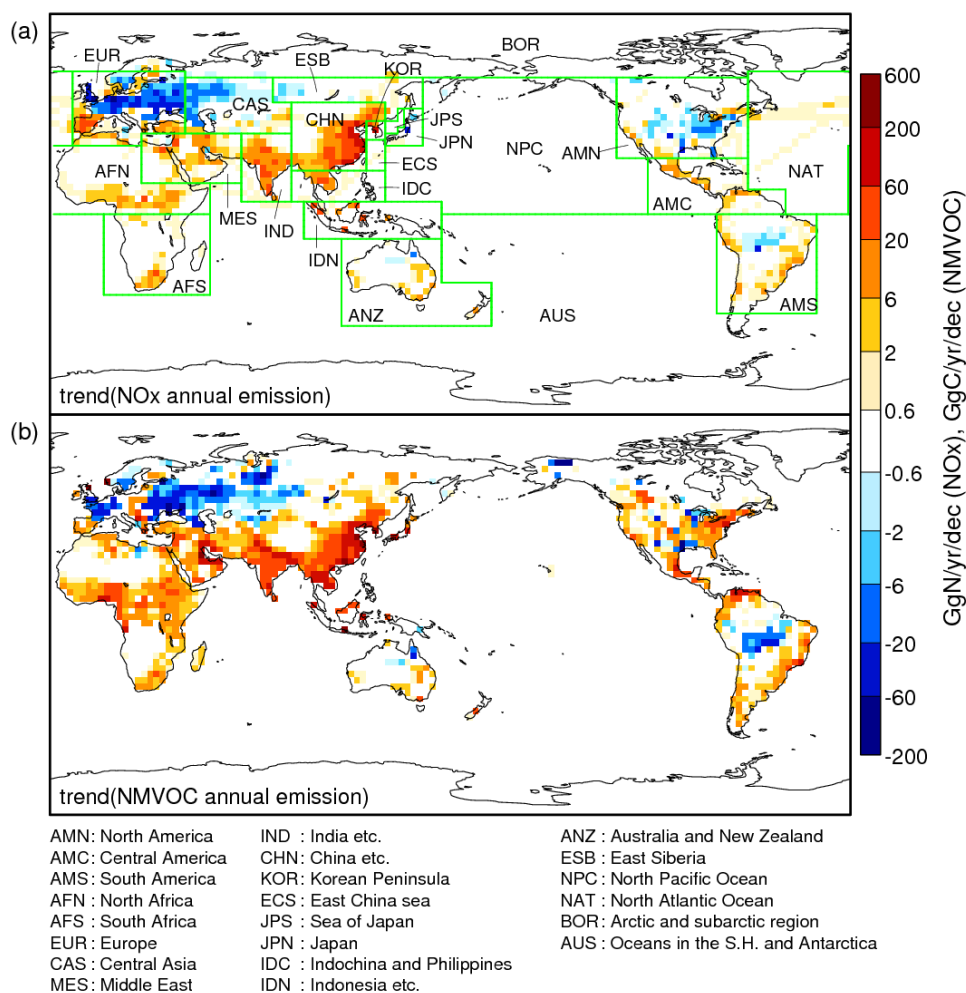
Figure 1. Linear trends of (a) NO_x and (b) NMVOC emission during the simulation period (1980–2005) used in the study. Significant trends at 5 % risk level are colored. Source regions for tracer tagging are also displayed in the top figure.

829
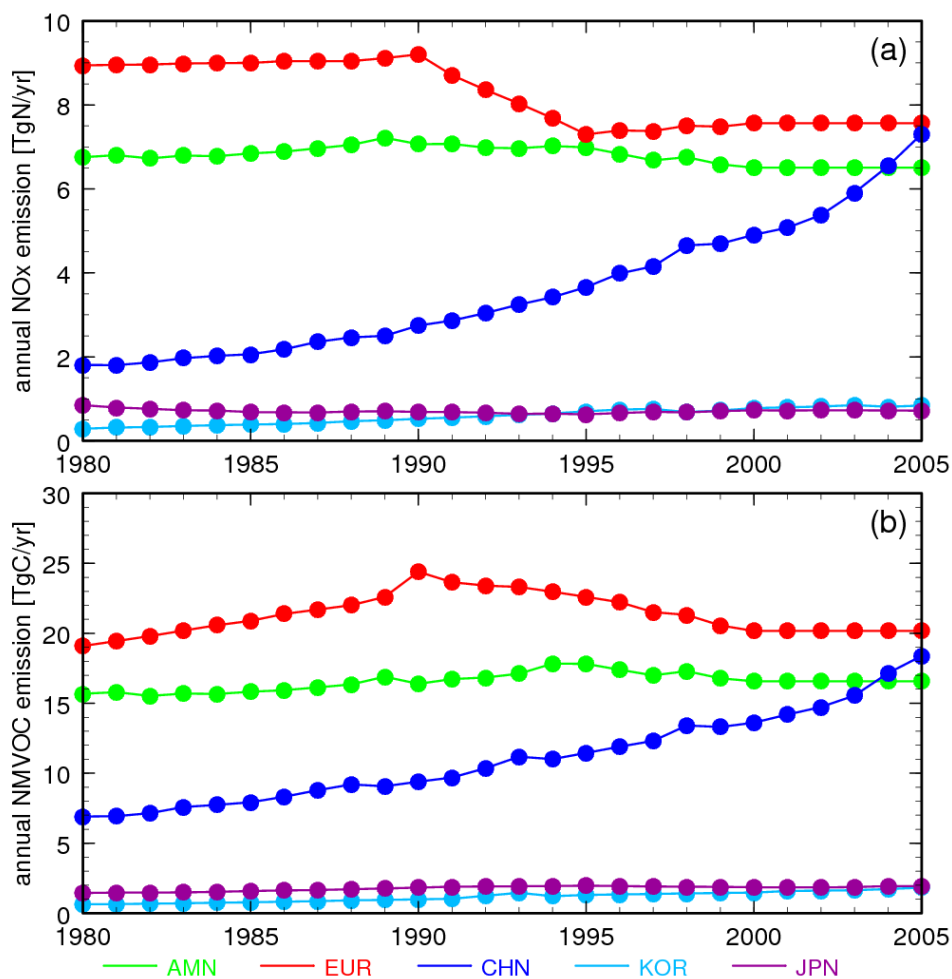
Figure 2. Temporal evolution of emissions of (a) NO$_x$ and (b) NMVOC averaged over several

831　source areas in the Northern Hemisphere depicted in Fig. 1.

Atmospheric
Chemistry
and Physics

Open Access

Discussions

EGU
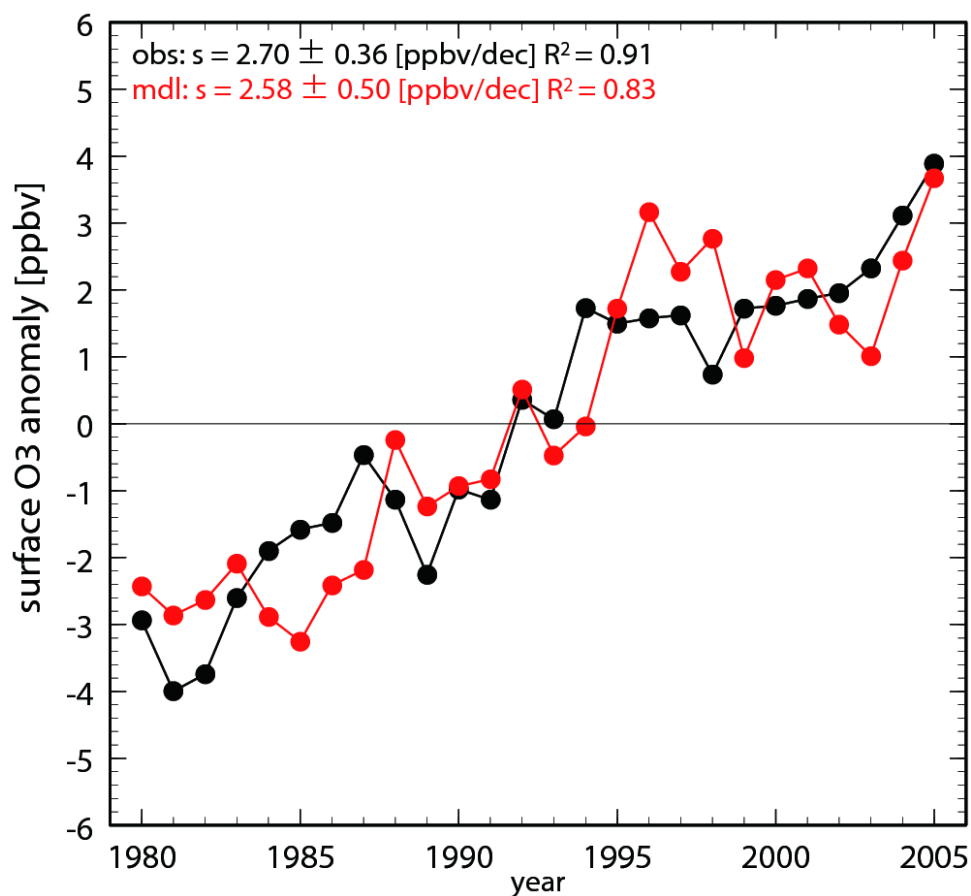
Figure 3. The temporal changes of annual mean surface O_3 anomaly averaged over Japan from observation (AEROS: black) and model calculation (red). Anomalies are defined as deviations from the values averaged over 1980–2005. The slope of a regression (s) for 1980–2005 with their 95 % confidence interval and R^2 are also shown.

Atmospheric
Chemistry
and Physics
Discussions
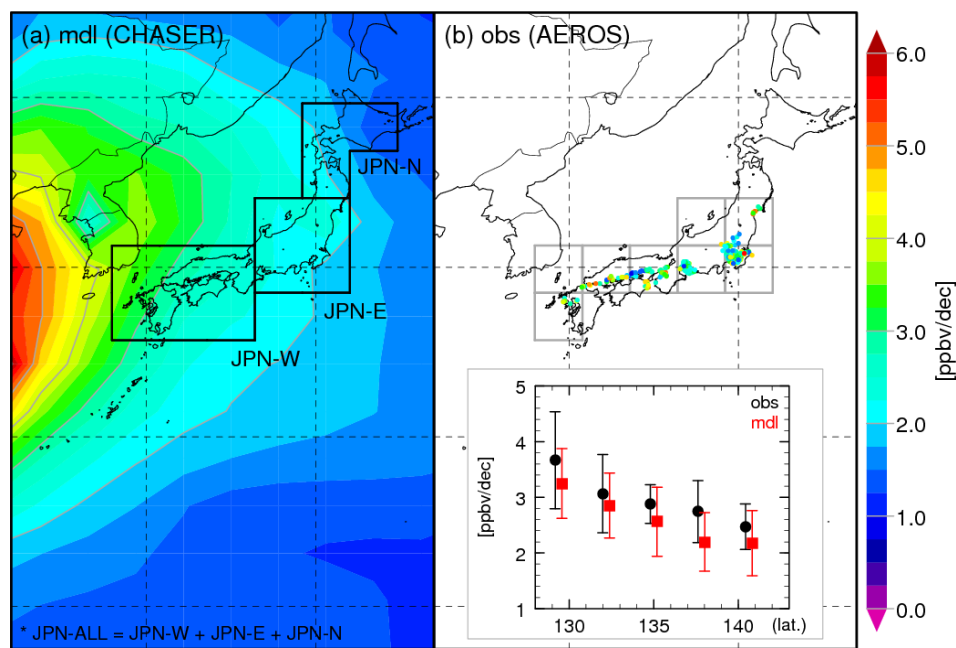
Figure 4. The linear trend of annual mean surface O_3 in 1980–2005 calculated from (a) model simulations and (b) observations at AEROS monitoring sites. The inset in figure (b) shows the longitudinal change of linear trends (black: AEROS observation; red: model) averaged within the model grids shown by gray rectangles. The error bars denote their 95 % confidence intervals. The black-rimmed areas in figure (a) are the area for averaging used in the figures from Fig. 6. Note that JPN-ALL is the sum of JPN-W, JPN-E, and JPN-N areas and used for the averaging in those figures.

Atmospheric
Chemistry
and Physics
Discussions

Open Access
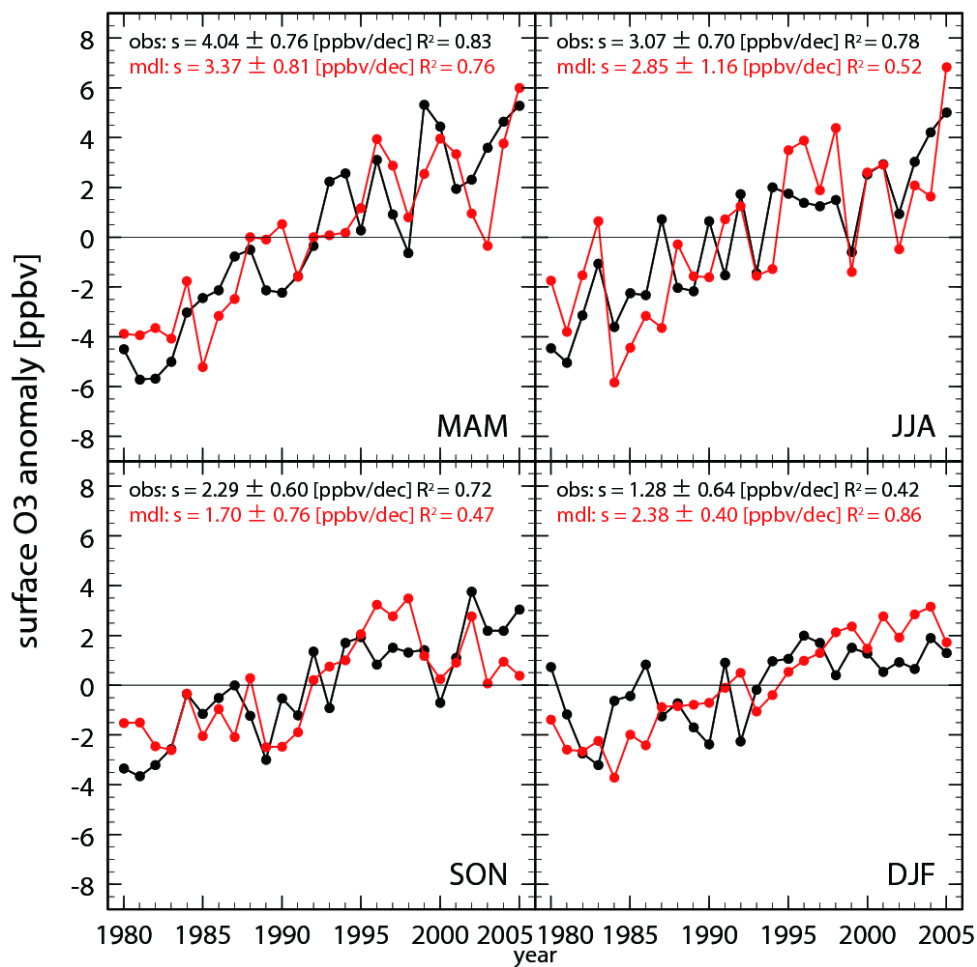
Figure 5. Same as Fig. 3 but the temporal changes of seasonal mean surface O_3 anomaly averaged over Japan from observations (AEROS: black) and model calculations (red).

28

848
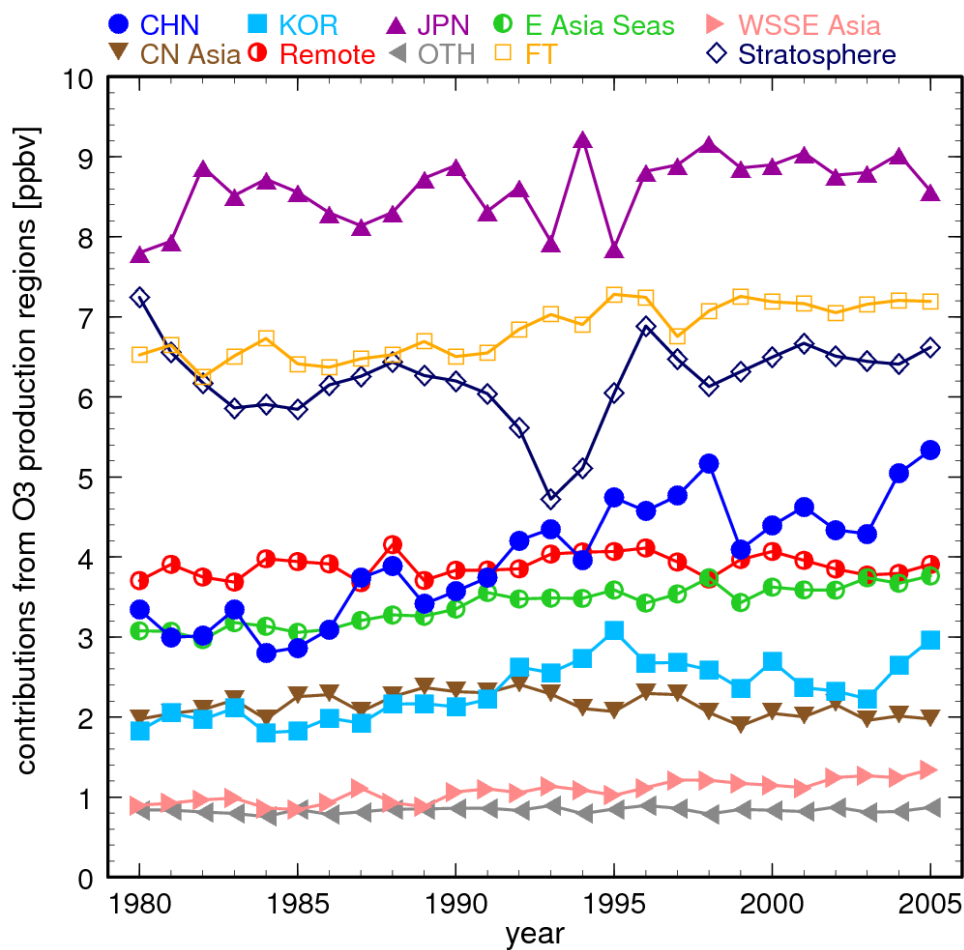
Figure 6. Long-term changes of annual mean contributions from source regions to surface O$_3$ over Japan. Some source regions are grouped: E-Asia-Seas is the sum of NPC, JPS, and ECS; WSSE Asia is the sum of MES, IND, IDN, and IDC; CN Asia is the sum of CAS and ESB; Remote is the sum of AMN, NAT, and EUR; and OTH is the other regions in the planetary boundary layer.

Atmospheric
Chemistry
and Physics
Discussions

854
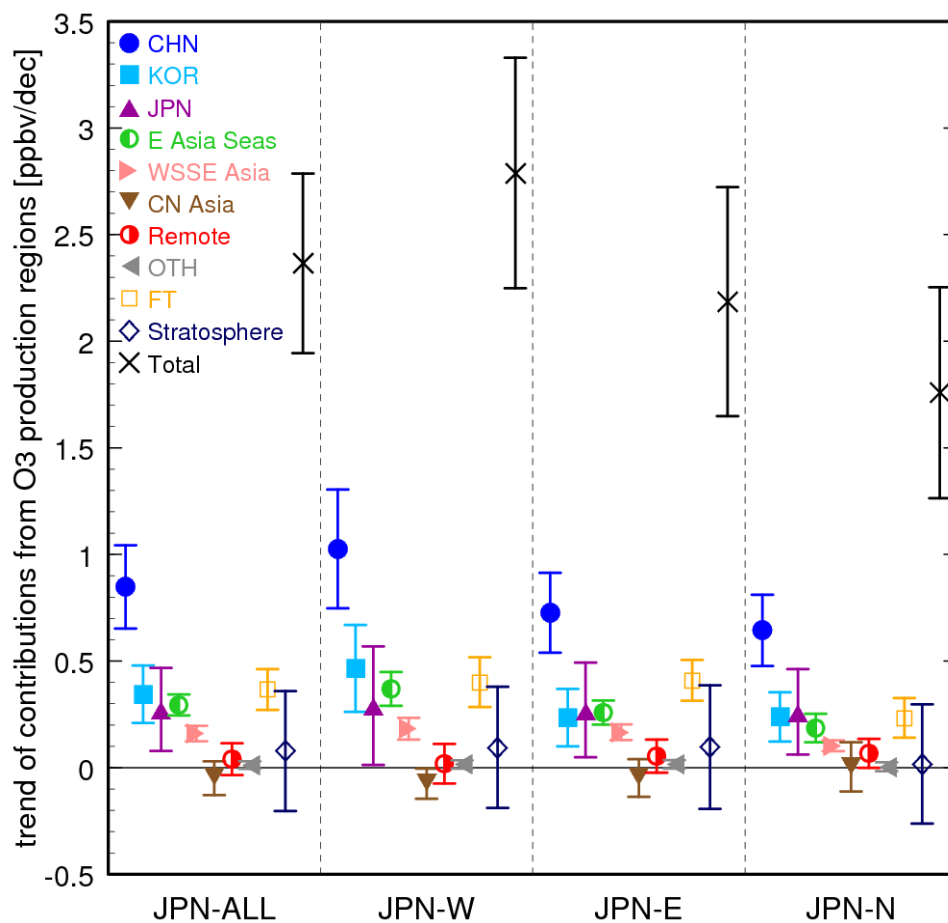
Figure 7. Linear trends of annual mean contributions in 1980–2005 from source regions to surface O_3 over Japan shown in Fig. 6 (JPN-ALL) and those averaged in three sub-regions in Japan (JPN-W, JPN-E, and JPN-N). Error bars are 95 % confidence intervals.

858
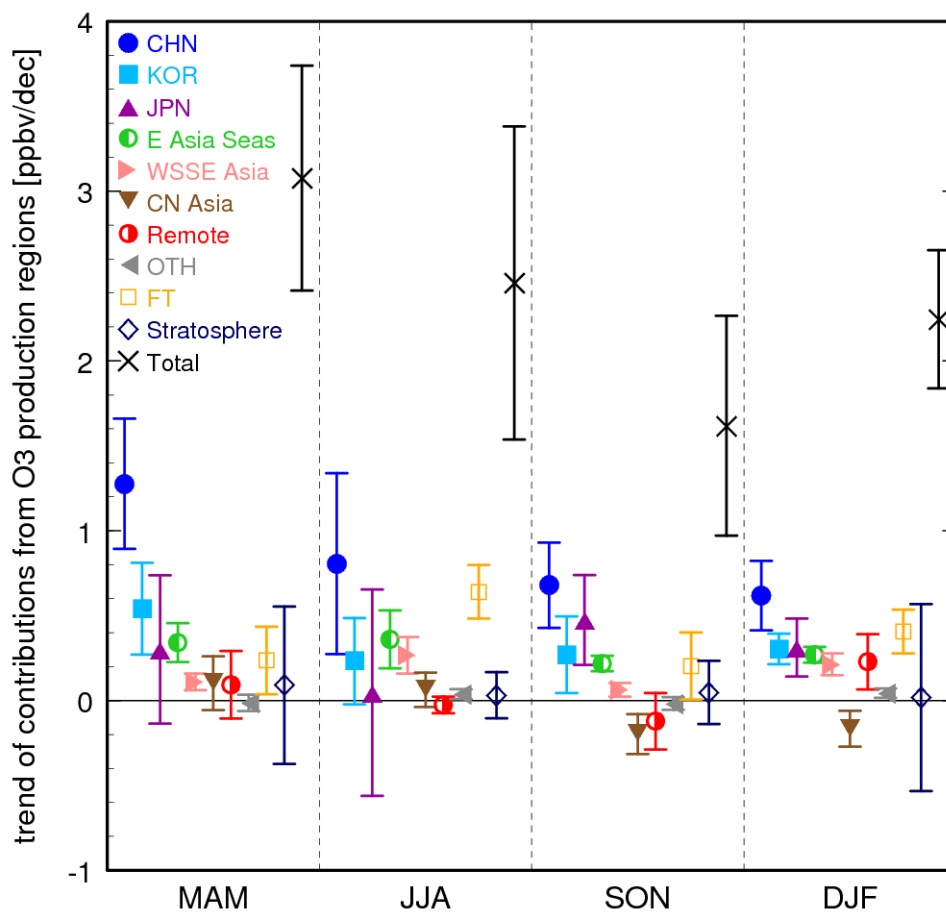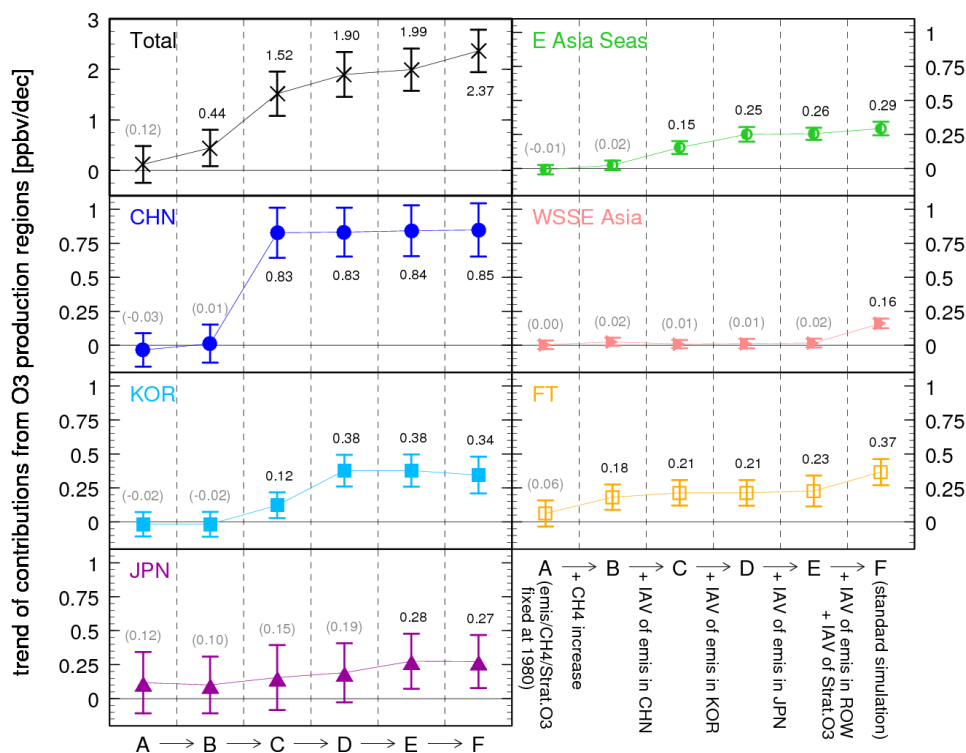
Figure 8. Linear trends of the contributions in 1980–2005 from source regions to surface O_3

over Japan in different seasons: spring (MAM), summer (JJA), fall (SON), and winter (DJF).

Error bars are 95 % confidence intervals.

Atmospheric
Chemistry
and Physics
Discussions

Open Access

Figure 9. Linear trends of the annual mean contributions in 1980–2005 from source regions to surface O_3 over Japan in the sensitivity simulations and the standard simulation (error bars are 95 % confidence intervals). The exact values of the trends are also shown in the figure; the trends without sufficient statistical significance are shown in parentheses. The trends of each region's contribution in the simulations A–E and F (the standard simulation) are arranged from left to right in each panel.